Polarization spectroscopy of $He^+(nl)$ produced in collisions of He^{2+} with H in Debye plasmas

L. Liu,[1,2] J. G. Wang,[2] and R. K. Janev[3]

[1]*College of Physical Sciences, Graduate University of the Chinese Academy of Sciences, P. O. Box 4588, Peoples Republic of China*

[2]*The Key Laboratory of Computational Physics, Institute of Applied Physics and Computational Mathematics, P. O. Box 100088, Peoples Republic of China*

[3]*Macedonian Academy of Sciences and Arts, P. O. Box 428, 1000 Skopje, Macedonia*

(Received 31 October 2010; published 31 January 2011)

Polarization spectroscopy of $He^+(nl)$ ion produced in He^{2+}-H(1s) collisions in a Debye plasma is studied by the two-center atomic orbital close-coupling (TC-AOCC) method in the energy range 1–200 keV/u. The atomic orbitals and electron binding energies of atomic states are calculated within the Debye-Hückel approximation of the screened Coulomb potential and used in the AOCC dynamics formalism to calculate the magnetic substate-selective electron-capture cross sections. It is demonstrated that the screening of Coulomb interactions affects the entire collision dynamics and the magnitude and energy behavior of m-state-selective cross sections. The changes in magnetic substate-selective electron-capture cross sections when the interaction screening varies introduce dramatic changes in the polarization spectroscopy with respect to the unscreened interaction case. The magnetic substate-selective electron-capture cross sections, as well as the polarization degrees for the $2p\ ^2P_{3/2}$–$1s\ ^2S_{1/2}$, $3p\ ^2P_{3/2}$–$2s\ ^2S_{1/2}$, $3d\ ^2D_{5/2}$–$2p\ ^2P_{3/2}$, and $3d\ ^2D_{3/2}$–$2p\ ^2P_{1/2}$ transitions in the He^+ ion produced in this collision system, are presented and discussed for a number of representative screening parameter values.

DOI: 10.1103/PhysRevA.83.012712 PACS number(s): 34.70.+e, 34.50.Fa, 34.20.Cf

I. INTRODUCTION

Electron capture by highly charged ions from neutral atoms and molecules has attracted much attention because of its wide applications in diverse fields of current interests. In this kind of process, the captured electron usually populates the excited states of the projectile ions that decay by line radiation. Due to the well-defined incident direction of the projectile, the emitted line may be polarized. The measurement of the polarization degree and angular distribution of emitted radiation are the only methods for observing the alignment of the final state produced by the electron capture which is determined by the population distribution of its magnetic substates. The information about the magnetic substate population allows one to probe the collision dynamics on a more fundamental level. Numerous experimental [1–8] and theoretical [9,10] studies have been devoted to the determination of photon polarization degree in collisions of multicharged ions with atoms and molecules. However, in the environment of hot dense plasmas, the Coulomb interaction between charged particles is screened which obviously affects the dynamics of atomic collision processes. Atomic collision processes in hot, dense plasmas play a crucial role in determining the radiation and transport properties of such plasmas and, therefore, have been subject to continuous interest during the last several decades. However, the studies involving heavy-particle collision processes in hot, dense plasmas are relatively scarce. The results of these studies are reviewed in [11–13]. Quite recently, we have performed extensive studies of the collision dynamics between hydrogen atom and fully stripped ions H^+ [14], He^{2+} [15,16], and O^{8+} [17] in Debye plasmas by employing the two-center atomic orbital close-coupling (TC-AOCC) method. In all the previously mentioned studies, however, the polarization degree of the radiation from excited capture states has not been investigated.

In the present work, we shall study the polarization degree of the $2p\ ^2P_{3/2}$–$1s\ ^2S_{1/2}$, $3p\ ^2P_{3/2}$–$2s\ ^2S_{1/2}$, $3d\ ^2D_{5/2}$–$2p\ ^2P_{3/2}$, and $3d\ ^2D_{3/2}$–$2p\ ^2P_{1/2}$ transitions in He^+ ion produced in He^{2+}-H collisions in a Debye plasma in the energy range 1–200 keV/u. The interaction between the active electron and H^+ and He^{2+} will be described by the Debye-Hückel potential,

$$V(r) = -\frac{Z}{r}e^{-r/r_d}, \tag{1}$$

with $Z = 1$ and $Z = 2$, respectively.

The Debye screening length r_d is related to the plasma electron temperature (T_e) and density (n_e) by $r_d = (k_B T_e/4\pi e^2 n_e)^{1/2}$, where k_B is the Boltzmann constant. The Debye potential is a good representation of the effective two-body electron-ion interaction as long as the Coulomb coupling parameter $\Gamma = e^2/(ak_BT_e)$ and plasma nonideality parameter $\gamma = e^2/(r_d k_B T_e)$ satisfy the conditions $\Gamma \leqslant 1, \gamma \ll 1$, where $a = [3/(4\pi n_e)]^{1/3}$ is the average interparticle distance. There is a wide class of laboratory and astrophysical plasmas in which these conditions are fulfilled (Debye plasmas).

We note that in the central-symmetric potential (1) the electron energy levels E_{nlm} are not degenerate in the orbital angular momentum quantum number l, but they still remain degenerate in the magnetic quantum number m [18]. Another important property of the potential (1) is that for any finite value of Debye length r_d it supports only a finite number of bound states. This implies that with decreasing r_d the energy E_{nl} of a bound nlm state decreases and enters in the continuum at certain critical screening length $r_{d,c}^{nl}$. For a given value of n, the energies of the states with higher l decrease faster and enter the continuum at larger $r_{d,c}^{nl}$ (see, e.g., [14–17]). Obviously, both the decrease of energies of the bound states with decreasing r_d and the reduction of their total number when r_d decreases affect the collision dynamics.

The capture dynamics in the studied $He^{2+} + H$ collision system will be described by the semiclassical TC-AOCC method, used also in our previous work on ion-atom inelastic

processes in Debye plasmas [14–17]. In the expansion basis, we shall include all states with $n \leqslant 7$ centered on He^+ and all states with $n \leqslant 3$ centered on H. In the energy range considered in our study, the TC-AOCC method should provide an adequate description of collision dynamics due to the large size of the expansion basis.

The paper is organized as follows. In Sec. II we briefly outline the theoretical method used in the calculations of cross sections and polarization degree. In Sec. III we present the results of our calculations for different values of screening length r_d and analyze the effects of the screening on the polarization degree. Finally, in Sec. IV we give our conclusions.

Atomic units will be used in the remaining part of this article, unless otherwise explicitly indicated.

II. THEORETICAL METHOD

A. Two-center atomic orbital close-coupling method

The application of the TC-AOCC method to an ion-atom collision system requires determination of single-center electronic states over which the total scattering wave function is expanded and used in a time-dependent Schrödinger equation to generate the coupled equations for the state amplitudes [19]. For determining the stationary bound electronic states with the potential (1) centered on the target ($Z = 1$) and on the projectile ($Z = 2$), we have used the variational method with the even-tempered trial functions [20],

$$\chi_{klm}(\vec{r};r_d) = N_l(\xi_k(r_d))r^l e^{-\xi_k(r_d)r} Y_{lm}(\hat{\vec{r}})\xi_k(r_d) = \alpha\beta^k, \quad k = 1,2,\ldots,N, \tag{2}$$

where $N_l(\xi_k)$ is a normalization constant, $Y_{lm}(\hat{\vec{r}})$ are the spherical harmonics, and α and β are variational parameters, determined by minimization of the energy for each value of r_d. The atomic states $\phi_{nlm}(\vec{r};r_d)$ are then obtained as the linear combination,

$$\phi_{nlm}(\vec{r};r_d) = \sum_k c_{nk}\chi_{klm}(\vec{r};r_d), \tag{3}$$

where the coefficients c_{nk} are determined by diagonalization of the single-center Hamiltonian. This diagonalization yields the energies $E_{nl}(r_d)$ of the atomic states in the screened Coulomb potential (1). In the collision energy range considered in the present paper (1–200 keV/u), the straight-line approximation for the relative nuclear motion, $R(t) = \vec{b} + \vec{v}t$ (b is the impact parameter and v is the collision velocity), can be safely adopted. Expanding the total electron wave function $\Psi(\vec{r},t)$ in terms of the bound atomic orbitals (3), multiplied by plane wave electron translational factors (ETFs),

$$\Psi(\vec{r},t) = \sum_i a_i(t)\phi_i^A(\vec{r},t;r_d) + \sum_j b_j(t)\phi_j^B(\vec{r},t;r_d), \tag{4}$$

and inserting it in the time-dependent Schrödinger equation $(H - i\frac{\partial}{\partial t})\Psi = 0$, where $H = -\frac{1}{2}\nabla_r^2 + V_A(r_A) + V_B(r_B)$, and $V_{A,B}(r_{A,B})$ are the electron interactions with the target proton and projectile ion He^{2+} of the form (1), one obtains the first-order coupled equations for the amplitude $a_i(t)$ and $b_j(t)$,

$$i(\dot{A} + S\dot{B}) = HA + KB, \tag{5a}$$

$$i(\dot{B} + S^\dagger\dot{A}) = \bar{K}A + \bar{H}B, \tag{5b}$$

where A and B are the vectors of the amplitudes a_i ($i = 1, 2, \ldots, N_A$) and b_j ($j = 1, 2, \ldots, N_B$), respectively. S is the overlap matrix ($S^\dagger$ is its transposed form), H and $\bar{H}$ are the direct coupling matrices, and K and $\bar{K}$ are the electron exchange matrices. The system of equations (5) is to be solved under the initial conditions,

$$a_i(-\infty) = \delta_{1i}, b_j(-\infty) = 0. \tag{6}$$

After solving the system of coupled equations (5), the cross section for $1 \to j$ electron-capture transition is calculated as

$$\sigma_{cx,j} = 2\pi\int_0^\infty |b_j(+\infty)|^2 bdb. \tag{7}$$

The sum of $\sigma_{cx,j}$ over j gives the corresponding total electron-capture cross section.

B. Degree of polarization

Taking the ion beam direction as the quantization axis, the degree of polarization of the radiation from an upper $|i\rangle$ to a lower $|f\rangle$ level is defined as

$$P = \frac{I_{//} - I_\perp}{I_{//} + I_\perp}, \tag{8}$$

where $I_{//}$ and $I_\perp$ are the photon intensities with the electric vector parallel and perpendicular to the ion beam direction, respectively. P can be expressed as a function of the alignment parameter A_0 by [21]

$$P = \frac{I_{//} - I_\perp}{I_{//} + I_\perp} = \frac{3h(j_i,j_f)A_0(j_i)}{4 + h(j_i,j_f)A_0(j_i)}, \tag{9}$$

where

$$h(j_i,j_f) = (-1)^{j_i - j_f}\begin{Bmatrix} j_i & j_i & 2 \\ 1 & 1 & j_f \end{Bmatrix}\begin{Bmatrix} j_i & j_i & 2 \\ 1 & 1 & j_i \end{Bmatrix}^{-1}, \tag{10}$$

and j_i and j_f are the total angular momenta of the initial and final state in the radiative transition, respectively. In the collision frame, the alignment parameter A_0 has the following form [21]:

$$A_0(j) = \frac{\sum_{mj}\{3m_j^2 - j(j+1)\}\sigma_{jm_j}}{j(j+1)\sum_{mj}\sigma_{jm_j}}. \tag{11}$$

Here σ_{jm_j} is the population of the (j, m_j) substate, which can be expressed in terms of the population of the (l, m) substate, σ_{lm}, using the Clebsch-Gordan coefficients,

$$\sigma_{jm_j} = \frac{1}{2}\sum_{m_l+m_s=m_j} |\langle lsm_lm_s|jm_j\rangle|^2\sigma_{lm}. \tag{12}$$

Due to the cylindrical symmetry about the beam axis, $\sigma_{lm} = \sigma_{l-m}$. Inserting (10)–(12) into (9), the resulting polarization degrees for the $2p\,^2P_{3/2}$–$1s\,^2S_{1/2}$, $3p\,^2P_{3/2}$–$2s\,^2S_{1/2}$, $3d\,^2D_{3/2}$–$2p$

$^2P_{1/2}$, $3d\ ^2D_{5/2}$–$2p\ ^2P_{3/2}$, and $3d\ ^2D_{3/2}$–$2p\ ^2P_{3/2}$ transitions are obtained as

$$P = \frac{3\tilde{\sigma}_{3/2,1/2} - 3\tilde{\sigma}_{3/2,3/2}}{5\tilde{\sigma}_{3/2,1/2} + 3\tilde{\sigma}_{3/2,3/2}} = \frac{6\sigma(3p_0) - 3\sigma(3p_1)}{10\sigma(3p_0) + 7\sigma(3p_1)}, \quad (13)$$

$$P = \frac{3\tilde{\sigma}_{3/2,1/2} - 3\tilde{\sigma}_{3/2,3/2}}{5\tilde{\sigma}_{3/2,1/2} + 3\tilde{\sigma}_{3/2,3/2}} = \frac{6\sigma(3d_0) + 3\sigma(3d_1) - 6\sigma(3d_2)}{10\sigma(3d_0) + 9\sigma(3d_1) + 6\sigma(3d_2)}, \quad (14)$$

$$P = \frac{\tilde{\sigma}_{5/2,3/2} + 4\tilde{\sigma}_{5/2,1/2} - 5\tilde{\sigma}_{5/2,5/2}}{5\tilde{\sigma}_{5/2,5/2} + 7\tilde{\sigma}_{5/2,3/2} + 8\tilde{\sigma}_{5/2,1/2}} = \frac{6\sigma(3d_0) + 3\sigma(3d_1) - 6\sigma(3d_2)}{12\sigma(3d_0) + 11\sigma(3d_1) + 8\sigma(3d_2)}, \quad (15)$$

$$P = \frac{3\tilde{\sigma}_{3/2,1/2} - 3\tilde{\sigma}_{3/2,3/2}}{4\tilde{\sigma}_{3/2,3/2} + 6\tilde{\sigma}_{3/2,1/2}} = \frac{6\sigma(3d_0) + 3\sigma(3d_1) - 6\sigma(3d_2)}{12\sigma(3d_0) + 11\sigma(3d_1) + 8\sigma(3d_2)}, \quad (16)$$

where $\tilde{\sigma}_{3/2,1/2} = \sigma_{3/2,+1/2} + \sigma_{3/2,-1/2}$, $\tilde{\sigma}_{3/2,3/2} = \sigma_{3/2,+3/2} + \sigma_{3/2,-3/2}$, $\tilde{\sigma}_{5/2,3/2} = \sigma_{5/2,+3/2} + \sigma_{5/2,-3/2}$, $\tilde{\sigma}_{5/2,1/2} = \sigma_{5/2,+1/2} + \sigma_{5/2,-1/2}$, $\tilde{\sigma}_{5/2,5/2} = \sigma_{5/2,+5/2} + \sigma_{5/2,-5/2}$, and $\sigma(2p_1) = \sigma(2p_{-1}) + \sigma(2p_{+1})$, $\sigma(3d_1) = \sigma(3d_{-1}) + \sigma(3d_{+1})$, $\sigma(3d_2) = \sigma(3d_{-2}) + \sigma(3d_{+2})$. Equation (13) combines the expressions for P for both $2p\ ^2P_{3/2}$–$1s\ ^2S_{1/2}$ and $3p\ ^2P_{3/2}$–$2s\ ^2S_{1/2}$ transitions. Because the cross sections for capture to the $n \geqslant 3$ states are much smaller than that of the $n = 2$ states in the entire energy range considered, the corresponding cascade contributions to $n = 2$ state populations can safely be neglected. A similar argument holds for the populations of $n = 3$ states. The populations of excited states are, thus, directly proportional to the electron-capture cross sections.

We note that the polarization degrees for the $3d\ ^2D_{5/2}$–$2p\ ^2P_{3/2}$ and $3d\ ^2D_{3/2}$–$2p\ ^2P_{3/2}$ transitions are the same, as indicated by the identity of Eqs. (15) and (16).

III. RESULTS FOR THE *m*-SELECTIVE CROSS SECTIONS AND POLARIZATION DEGREES

A. $2p\ ^2P_{3/2}$–$1s\ ^2S_{1/2}$ transition

As mentioned in Sec. II A, in solving the coupled-channel equations (5) all $n \leqslant 7$ states centered on He^+ and all $n \leqslant 3$ states centered on H have been used in the expansion basis. We first check the sufficiency of adopted basis from the point of view of reliability of calculated cross sections for the case of unscreened Coulomb interaction. As expected from the analysis and calculations performed in Ref. [22], even the more restricted basis ($n \leqslant 4$ states on He^+ and $n \leqslant 3$ states on H) provides an acceptable description of electron-capture dynamics for this collision system in the unscreened case. The cross sections for electron capture to the $1s$, $2s$, and $2p$ states of He^+ ion in the zero-screening case are shown in Fig. 1 and compared with the results of previous TC-AOCC calculations of Ref. [22] (denoted by crosses). It can be seen that the present calculations coincide with those of Ref. [22] in the overlapping energy range. The cross sections for capture to the higher nl states also have the same level of mutual agreement. We note, however, that for the case of screened Coulomb interaction the convergence of results appears to be somewhat slower, which prompted us to use a larger basis on He^+.

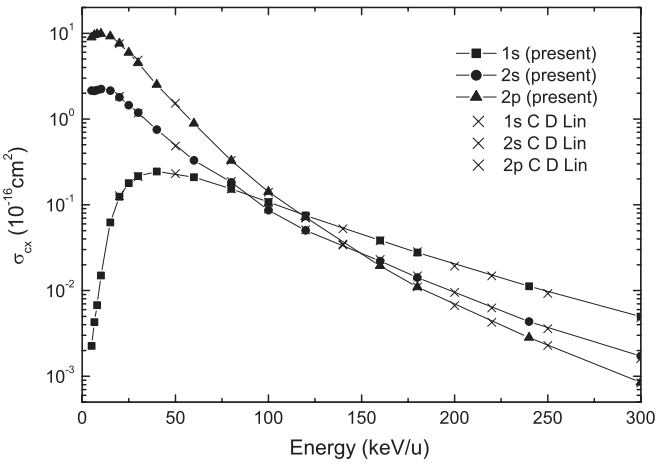

FIG. 1. Cross sections for electron capture to $1s$, $2s$, and $2p$ states of He^+; the crosses are the results of Ref. [22].

In Fig. 2 we present the energy dependence of magnetic substate-selective cross sections for electron capture to $2p_0$ [panel (a)] and $2p_1$ [panel (b)] states of the He^+ ion for the unscreened case and screened cases with $r_d = 12, 8, 6$, and $4a_0$.

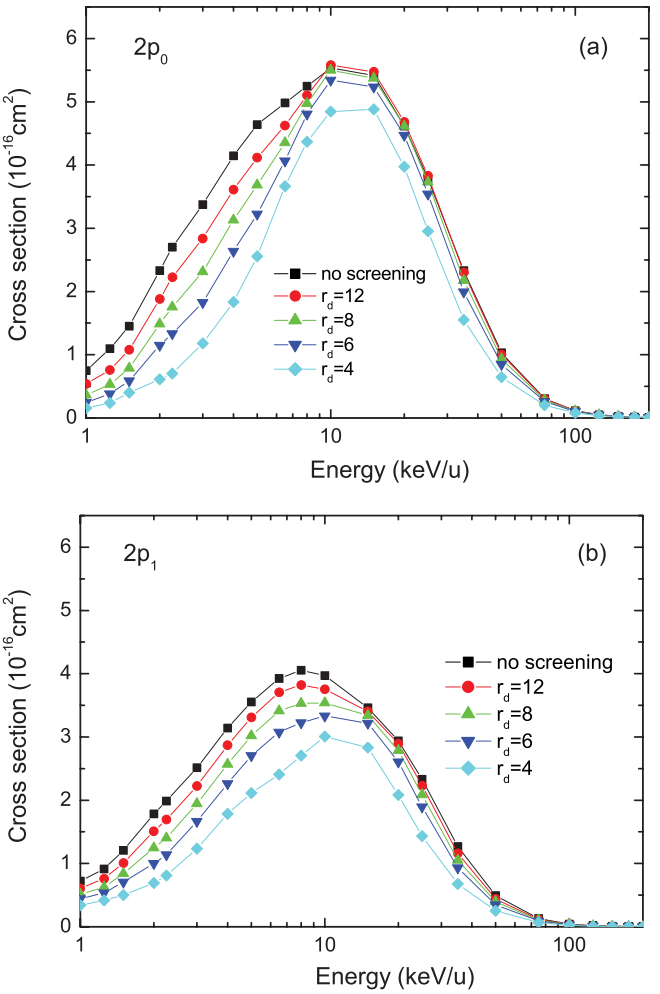

FIG. 2. (Color online) Cross sections for electron capture to $2p_0$ (a) and $2p_1$ (b) states of He^+ ion for the unscreened case and screened cases with $r_d = 12$, 8, 6, and $4a_0$.

As discussed in Ref. [15], the $2p$ electron-capture channel is the dominant channel for this collision system also in the screened case. The m-partial cross sections for the $2p$ state have similar energy behavior in the considered energy range when r_d varies. With decreasing r_d, the cross sections for capture to $2p_0$ and $2p_1$ also decrease. This behavior of m-partial cross sections is a direct consequence of the decrease of electron exchange matrix elements with decreasing r_d [15]. It is important to note in these figures that in the low-energy region (below $\sim$12 keV/u) the relative decrease of the $\sigma(2p_0)$ cross section with decreasing the energy is faster than that for $\sigma(2p_1)$. In contrast to this, in the energy region above $\sim$10–12 keV/u the relative decrease of the $\sigma(2p_1)$ cross section with increasing the energy is faster than that for $\sigma(2p_0)$, but the decrease of both partial cross sections with decreasing r_d is much less pronounced than in the region below $\sim$10–12 keV/u. It is also worth noting that while the energy position of the maximum of $\sigma(2p_0)$ cross section does not change markedly with varying r_d, that for the $\sigma(2p_1)$ cross section increases when r_d decreases. As mentioned earlier, the differences in the r_d behavior of the $\sigma(2p_{0,1})$ cross sections are related to the differences in the corresponding coupling matrix elements. The different energy and r_d behavior of the $\sigma(2p_{0,1})$ cross sections below and above $\sim$10–12 keV/u will, according to Eq. (13), obviously be reflected in the E and r_d behavior of the polarization degree.

In Fig. 3 we present the energy behavior of the polarization degree for the $2p\ ^2P_{3/2}$–$1s\ ^2S_{1/2}$ transition in the He^+ ion produced in He^{2+}-H collisions for the unscreened case and screened cases with $r_d = 12$, 8, 6, and $4a_0$. As mentioned earlier, in this collision system the $2l$ capture states are the dominantly populated ones (due to their energy quasiresonance with the initial state) in the considered energy range so that the radiative cascade contributions from the higher nl states can be neglected. It can be seen from this figure that in the zero-screening case, the polarization degree shows a mild maximum in the energy region 2–4 keV/u, similarly as in the case of $N^{4+}(3p\ ^2P_{3/2}$–$3s\ ^2S_{1/2})$ produced in N^{5+}-He and

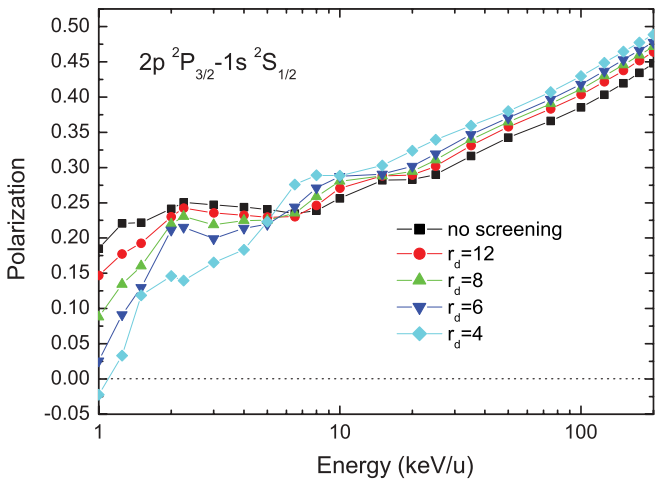

FIG. 3. (Color online) Degree of polarization of the line corresponding to the $2p\ ^2P_{3/2}$–$1s\ ^2S_{1/2}$ transition in He^+ as a function of projectile energy for the unscreened case and screened cases with $r_d = 12$, 8, 6, and $4a_0$.

N^{5+}-H_2 collisions, which has been experimentally observed in Ref. [8] and theoretically analyzed in Ref. [9]. As we see from Fig. 3, in the case of a considerable interaction screening ($r_d \leqslant 12a_0$), this maximum disappears. The polarization degree in the screened case in Fig. 3 exhibits two prominent features: (i) it monotonically increases with increasing energy in the considered energy range, and (ii) for energies below $\sim$6 keV/u it decreases with decreasing r_d, while for energies above $\sim$6 keV/u it increases with decreasing r_d. The first feature is a result of the fact that the cross section $\sigma(2p_0)$ is larger than $\sigma(2p_1)$ in the entire energy range considered for all considered values of r_d (see Fig. 2), while the second feature is a result from the interchange of the rate of relative decrease of $\sigma(2p_0)$ and $\sigma(2p_1)$ at $\sim$10–12 keV/u with decreasing r_d, as discussed earlier. This E and r_d behavior of the polarization degree P for this transition follows directly from Eq. (13): the strong decrease of P with decreasing r_d below $\sim$6 keV/u (especially below $\sim$2 keV/u) reflects the similarly strong decrease of $\sigma(2p_0)$ in the region below $\sim$12 keV/u [see Fig. 2(a)], while the more gradual increase of P with decreasing r_d in the energy region above $\sim$6 keV/u is a consequence of the similar increase of the difference $\sigma(2p_0)$-$\sigma(2p_1)$ in the region above $\sim$12 keV/u [compare Figs. 2(a) and 2(b)]. We note that the increase of P with increasing energy in the high-energy region is a consequence of the fact that the cross section for capture to a nlm state decreases faster with increasing energy when m increases (see, e.g., [23,24]). The increase of P with increasing energy is, however, limited and in the present case its limiting value is 0.6, as it follows from Eq. (13). It is worth noting that the values of the polarization degree for $r_d = 4a_0$ become negative for $E \sim 1$ keV/u.

B. $3p\ ^2P_{3/2}$–$2s\ ^2S_{1/2}$ transition

The energy dependences of $3p_0$ and $3p_1$ state-selective cross sections for the unscreened case and for the screened cases with $r_d = 12a_0$, $8a_0$, and $6a_0$ are shown in Figs. 4(a) and 4(b), respectively. We note that for $r_d = 4a_0$, the $3p_m$ states of He^+ are already in the continuum. As observed in Fig. 4, the $\sigma(3p_{0,1})$ partial cross sections for both the unscreened and screened cases have a quite different energy behavior than the $\sigma(2p_{0,1})$ cross sections and are about an order of magnitude smaller (see Fig. 2). These differences in the $\sigma(3p_{0,1})$ and $\sigma(2p_{0,1})$ cross sections are understandable if one takes into account the energy quasiresonance of the initial $H(1s)$ state with the final $He^+(2p)$ state (that holds even in the screened case down to very small Debye lengths), which in the case of the $He^+(3p)$ state is destroyed. The increased reaction energy defect in the case of capture to $3p_{0,1}$ states shifts the maxima of the $\sigma(3p_{0,1})$ cross sections to $\sim$25–30 keV/u [as opposed to $\sim$10–12 keV/u for $\sigma(2p_{0,1})$; see Figs. 2 and 4]. In addition, the dynamics involved in the capture to $3p_{0,1}$ states produces new secondary cross-section maxima in the $\sigma(3p_{0,1})$ cross sections in the energy region $\sim$3–5 keV/u (for both the unscreened and screened cases). In the case of $\sigma(3p_0)$ these secondary maxima are relatively small but in the case of $\sigma(3p_1)$ they become comparable with the high-energy maxima. It is interesting to note in Figs. 4(a) and 4(b) that while the values of low-energy maxima of $\sigma(3p_0)$ cross sections in the screened cases are

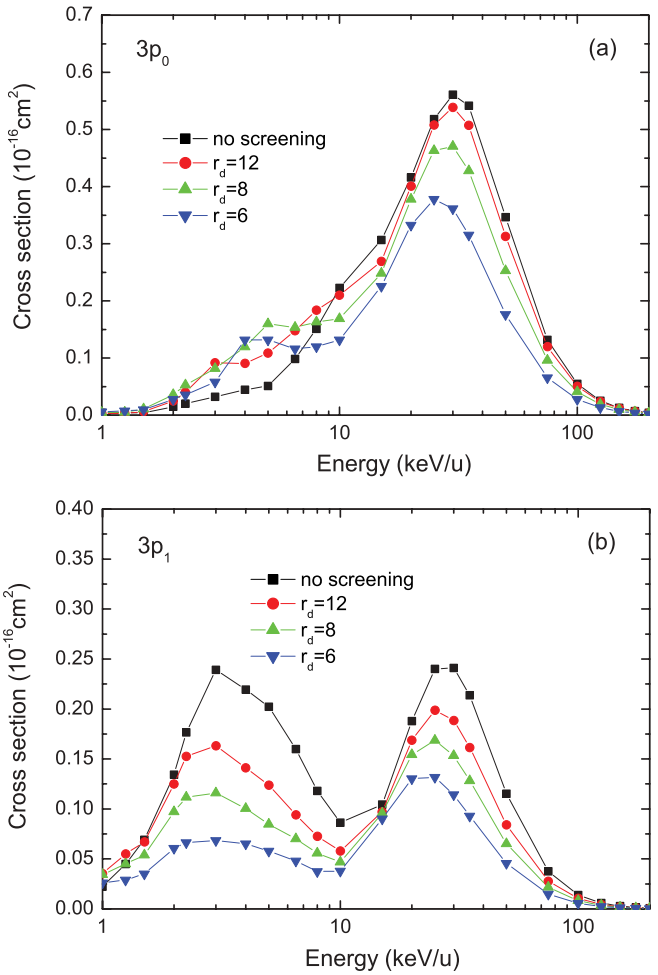

FIG. 4. (Color online) Cross sections for electron capture to $3p_0$ (a) and $3p_1$ (b) states of He^+ in the He^{2+}-H collision.

larger than that for the unscreened case (without showing a clear regularity of increase with decreasing r_d), those of the $\sigma(3p_1)$ cross sections are smaller than the one for the unscreened case and decrease with decreasing r_d. A detailed analysis of the mutual couplings between the $He^+(n = 2)$, $H(n = 2)$, and $He^+(n = 3)$ states has revealed that the population of $He^+(3p_1)$ at low collision energies is dominated by the $H(2s_0)$-$He^+(3p_1)$ coupling which decreases with decreasing r_d. In a molecular picture of the collision dynamics this would correspond to the rotational $3p\sigma$-$3p\pi$ coupling in the united atom region. Within the same dynamical picture, the $He^+(3p_1)$ state in the receding stage of the collision becomes subject to a Stark mixing with the state $He^+(3p_0)$ due to the electric field of the H^+ ion. This reduces the population of the $He^+(3p_1)$ state, but leads to an increase of the population of the $He^+(3p_0)$ asymptotic state in the same energy region, as observed in Fig. 4(a).

The degree of polarization of the emission line corresponding to the $3p\ ^2P_{3/2}$–$2s\ ^2S_{1/2}$ transition in He^+ is shown in Fig. 5 as a function of the projectile energy for the unscreened case and for interaction screening with $r_d = 12$, 8, and $6a_0$. As expected on the basis of the difference of the m-selective capture cross sections $\sigma(2p_{0,1})$ and $\sigma(3p_{0,1})$ (cf. Figs. 2 and 4), both the energy and r_d dependences of the polarization

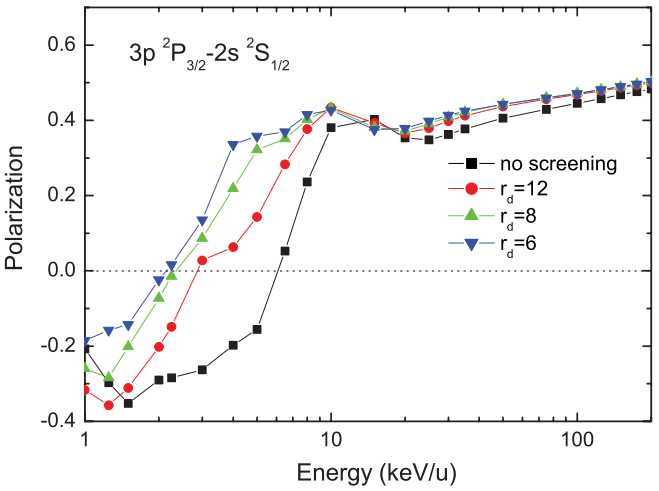

FIG. 5. (Color online) Polarization degree of the line corresponding to the $3p\ ^2P_{3/2}$–$2s\ ^2S_{1/2}$ transition in He^+ as a function of projectile energy for the unscreened case and screened cases with $r_d = 12$, 8, and $6a_0$.

degree for the $3p\ ^2P_{3/2}$–$2s\ ^2S_{1/2}$ transition are considerably different from those for the $2p\ ^2P_{3/2}$–$1s\ ^2S_{1/2}$ transition, particularly in the low-energy region (compare Figs. 3 and 5). With decreasing r_d, the polarization degree P in Fig. 5 increases with respect to the unscreened case in the entire energy range considered (except for the region below ~1.5 keV/u). This increase of P is much more pronounced in the energy region below ~10 keV/u than at higher energies, where it tends to diminish with increasing the energy. The reduced sensitivity of P on r_d in the energy region above ~10 keV/u reflects the comparable degree of relative decrease of the $\sigma(3p_0)$ and $\sigma(3p_1)$ cross sections for energies above ~25 keV when r_d varies (see Fig. 4). Physically, this is a result of the increased role of momentum transfer mechanism (and not the reaction energy defect) in the electron-capture dynamics and the predominance of the capture to the $m = 0$ state within the lm manifold at high energies [23,24]. It is also worth noting that the polarization degree for this transition becomes negative in the energy region below ~10 keV/u, the change of its sign appearing at energies decreasing with decreasing r_d. All the E and r_d variations of the polarization degree, observed in Fig. 5, obviously follow directly from the corresponding variations of the $\sigma(3p_{0,1})$ cross sections and their combination in the expression (13) for P.

We have specifically investigated the role of cascade contributions from the $n = 4,5$ states to the population of $3p_{0,1}$ states. We have found that even at the high energies ($E = 100$, 200 keV/u) these contributions change the value of P by less than 1%.

C. $3d\ ^2D_{3/2}$–$2p\ ^2P_{1/2}$ and $3d\ ^2D_{5/2}$–$2p\ ^2P_{3/2}$ transitions

The energy dependences of the cross sections for electron capture to the $3d_0$, $3d_1$, and $3d_2$ states of He^+ ion for the unscreened case and for interaction screening with $r_d = 12a_0$, $8a_0$, and $6a_0$ are shown in panels (a)–(c) of Fig. 6, respectively. Like in the case of electron capture to $3pm$ states, the cross sections for capture to $3dm$ states are an order of magnitude

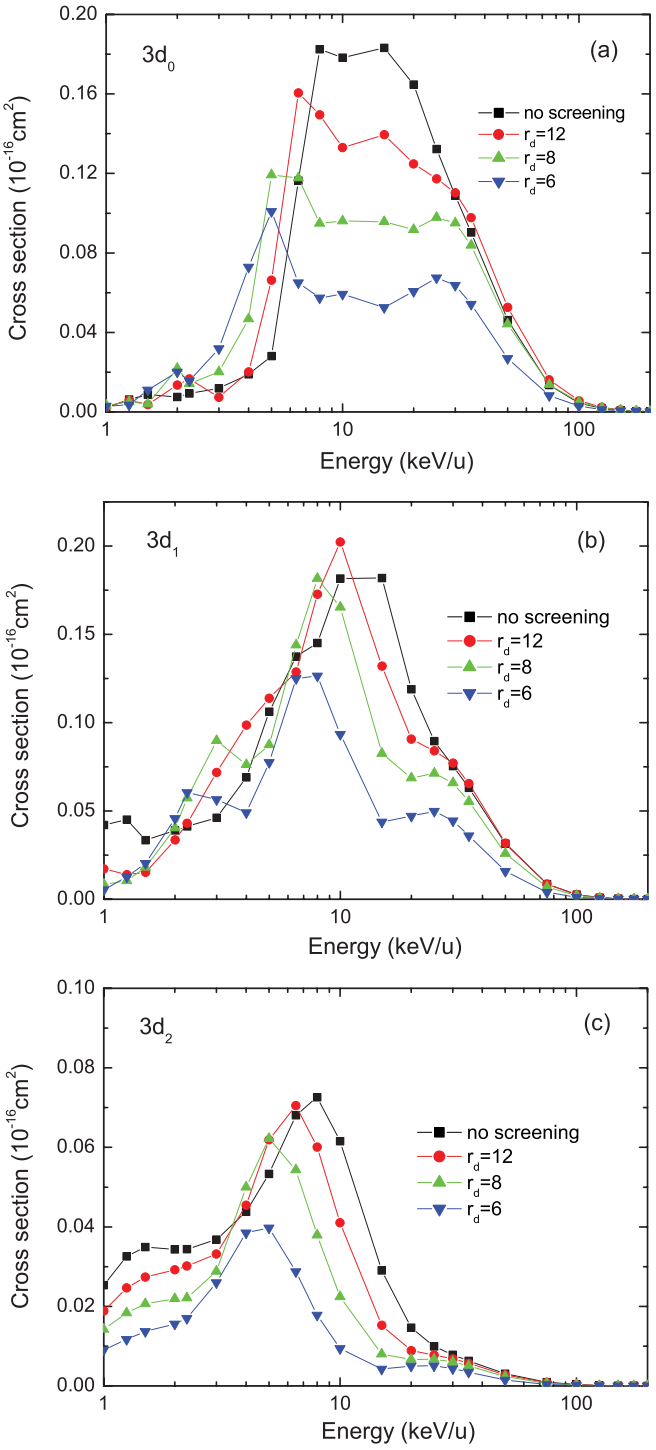

FIG. 6. (Color online) Cross sections for electron capture to $3d_0$ (a), $3d_1$ (b), and $3d_2$ (c) states of He^+ in the He^{2+}-H collision.

smaller than those for capture to $2pm$ states for the same reasons as those discussed in connection with the smallness of $3pm$ cross sections (see previous subsection). The energy and r_d behavior of the $\sigma(3d_{0,1,2})$ cross sections observed in Figs. 6(a)–6(c) differ considerably when m changes. The $\sigma(3d_0)$ cross section for the unscreened case has a maximum at ~8 keV/u; above this energy the cross section first decreases slowly, exhibits a small increase in the range ~12–15 keV/u, and then attains its typical high-energy decrease. For energies below its maximum this cross section drops steeply and has a small secondary maximum at ~2 keV/u. The $\sigma(3d_0)$ cross sections for the screened cases exhibit oscillatory structures in the energy range (roughly) ~5–30 keV/u; above and below the oscillatory domain they decrease. The maxima of these structures move toward the lower energies when r_d decreases and this is the main reason for the increase of the cross section with decreasing r_d, observed in the low-energy region. A small secondary maximum at ~2 keV/u appears also in the cross sections for the screened cases. It should be noted in Fig. 6(a) that in the energy range where the oscillatory structures of the $\sigma(3d_0)$ cross sections in the screened cases appear their decrease with decreasing r_d is very strong. At energies above this energy range, the decrease of $\sigma(3d_0)$ with decreasing r_d is much slower. [The apparent larger $\sigma(3d_0)$ cross section for $r_d = 12a_0$ than that for the unscreened case in the region above ~30 keV/u is a result of the insufficiently large expansion basis on He^+ in this case.] The $\sigma(3d_1)$ cross sections in Fig. 6(b) show a significantly different E and r_d behavior than that for $\sigma(3d_0)$: on both sides of the central cross-section maxima (occurring in the energy range ~6–12 keV/u) additional secondary maxima are observed. The positions of high-energy secondary maxima are all in the region of $E \sim 25$ keV/u, while those of the low-energy maxima are distributed between $E \sim 6$ keV/u (for the unscreened case) and $E \sim 2.5$ keV/u (for $r_d = 6a_0$). It should be noted in Fig. 6(b) that while in the energy regions above the energy positions of the central cross-section maxima the $\sigma(3d_1)$ cross section decreases with decreasing r_d, its r_d behavior below these energies becomes irregular. This is mainly due to the shifts of the central and low-energy peaks in the cross sections toward the lower energies when r_d decreases. The shift of the cross-section structure toward lower energies both in $\sigma(3d_0)$ and $\sigma(3d_1)$ in the energy region below $E \sim 15$ keV/u with decreasing r_d is related to a large extent to the decrease of the energy defect between the final and initial states in the capture process when r_d decreases [14–17]. The cross sections $\sigma(3d_2)$ shown in Fig. 6(c) show roughly a similar E and r_d behavior like the $\sigma(3d_1)$ cross sections in Fig. 6(b) except that the high-energy ($E \sim 25$ keV/u) cross-section maxima in the screened cases are now much smaller and, in the energy region below $E \sim 3$ keV/u, the cross section shows a regular decrease with decreasing r_d. It is worth noting that the $\sigma(3d_2)$ cross sections are about a factor of two smaller than the corresponding $\sigma(3d_1)$ cross sections, a result routed in the fact that (in the molecular picture of collision dynamics) the $l\pi \rightarrow l\delta$ rotational coupling in the united atom region is significantly weaker than the $l\sigma \rightarrow l\pi$ rotational coupling. The diversity of the E and r_d behavior of the $\sigma(3d_{0,1,2})$ cross sections in the considered E and r_d ranges indicates the complexity of the capture dynamics leading to the population of $3d_{0,1,2}$ states.

Figure 7 shows the energy behavior of the polarization degree of the lines corresponding to the $3d\ ^2D_{3/2}$–$2p\ ^2P_{1/2}$ [panel (a)] and $3d\ ^2D_{5/2}$–$2p\ ^2P_{3/2}$ [panel (b)] transitions in He^+ for the unscreened case and for the screened cases with $r_d = 12a_0$, $8a_0$, and $6a_0$. As mentioned in Sec. II B, the polarization degree of the $3d\ ^2D_{3/2}$–$2p\ ^2P_{3/2}$ transition is the same as that for the $3d\ ^2D_{5/2}$–$2p\ ^2P_{3/2}$ transition. It is surprising to see in Figs. 7(a) and 7(b) that the calculated polarization degrees for

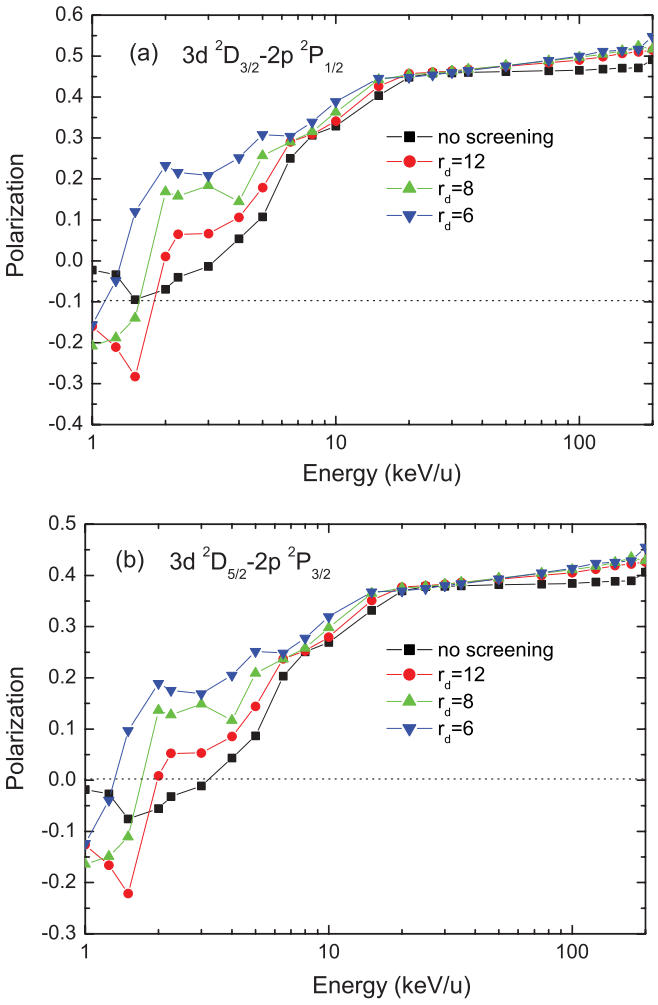

FIG. 7. (Color online) Degree of polarization of the lines corresponding to $3d\,^2D_{3/2}$–$2p\,^2P_{1/2}$ (a) and $3d\,^2D_{5/2}$–$2p\,^2P_{3/2}$ (b) transitions in He^+ as a function of projectile energy for the unscreened case and for screened cases with $r_d = 12$, 8, and $6a_0$.

the $3d\,^2D_{3/2}$–$2p\,^2P_{1/2}$ and $3d\,^2D_{5/2}$–$2p\,^2P_{3/2}$ transitions exhibit a very similar energy behavior in both the unscreened and screened cases, despite the variety of E and r_d behavior of the $3dm$ capture cross sections observed in Figs. 6(a)–6(c). The magnitude of the polarization degree for the $3d\,^2D_{3/2}$–$2p\,^2P_{1/2}$ transition is, however, considerably larger than that for the $^2D_{5/2}$–$2p\,^2P_{3/2}$ transition. It is worth nothing that in the entire energy region considered, the polarization degree increases with decreasing r_d and that, except for $r_d = 6a_0$, it becomes negative at low energies for both transitions. We further note that, according to Eqs. (14) and (15), the high-energy limits of P for the $3d\,^2D_{3/2}$–$2p\,^2P_{1/2}$ and $3d\,^2D_{5/2}$–$2p\,^2P_{3/2}$ transitions are 0.6 and 0.5, respectively.

IV. CONCLUSIONS

In the present work we have investigated the polarization spectroscopy of the $He^+(nl)$ ion produced in He^{2+}-H(1s) collisions in a Debye plasma. The collision dynamics in the energy range 1–200 keV/u was described by the semiclassical TC-AOCC method. The AO expansion basis used in the present study included all $n \leqslant 7$ states on He^+ and all $n \leqslant 3$ states on the H atom and was found to be well convergent even for the weak capture channels in the energy range considered. We have calculated the state-selective $2p_{0,1}$, $3p_{0,1}$, and $3d_{0,1,2}$ electron-capture cross sections for the unscreened case and for the screened cases with Debye lengths $r_d = 12$, 8, $6a_0$ (and $r_d = 4a_0$ for $2p_{0,1}$) required to calculate the polarization degree of the radiation corresponding to the transitions $2p\,^2P_{3/2}$–$1s\,^2S_{1/2}$, $3p\,^2P_{3/2}$–$2s\,^2S_{1/2}$, $3d\,^2D_{5/2}$–$2p\,^2P_{3/2}$, and $3d\,^2D_{3/2}$–$2p\,^2P_{1/2}$ in He^+ [cf. Eqs. (13)–(16)]. Due to the large difference between the nlm cross sections for $n = 2$ and $n = 3$, and (to a lesser extent) between those for $n = 3$ and $n = 4$, the radiative cascade contributions to the population of the upper state in the previously mentioned transitions were considered as negligible.

The m-selective capture cross sections, displayed in Figs. 2, 4, and 6, were found to be rather sensitive to the strength of interaction screening: while in the intermediate and high-energy region the interaction screening results in a decrease of the cross section, in the low-energy region the effect of the screening may lead also to its increase. Significant variations of m-selective cross sections have been observed in their energy dependence as well, particularly in the low-energy region. As demonstrated in our previous work for the unscreened case [9] (see also [25]), the energy behavior of the m-selective cross section is dominantly affected by the rotational coupling in the united atom region and by the Stark mixing of lm states (within a given n manifold) at large internuclear distances by the field of residual ion. These mechanisms of redistribution of the m-state populations in the course of the collision remain basically the same when the interaction is screened. As Figs. 2, 4, and 6 demonstrate, the interaction screening introduces significant changes in the collision dynamics by affecting the electron binding energies and couplings between the states (the moduli of both of which decrease with increasing the strength of the screening).

The polarization degree P of the emitted light for the considered transitions exhibits a similar sensitivity to the strength of the screening, particularly at the low collision energies. For energies below $E \sim 6$ keV/u, the polarization degree for the $2p\,^2P_{3/2}$–$1s\,^2S_{1/2}$ transition decreases with increasing the screening, while for the higher energies it increases (cf. Fig. 3). For all other studied transitions, P increases with increasing the screening in the entire energy range considered (except for the small energy region around $E \sim 12$ keV/u in the case of the $3p\,^2P_{3/2}$–$2s\,^2S_{1/2}$ transition; see Fig. 5). It should be noted that while the differences in P for different values of the screening are quite significant in the low-energy region (below $E \sim 4$ keV/u for $2p\,^2P_{3/2}$–$1s\,^2S_{1/2}$ and below $E \sim 10$ keV/u for the other transitions), they become relatively small at the high energies. The weak high-energy sensitivity of P to the interaction screening results from two facts: the increased role of the momentum transfer mechanism in electron-capture dynamics and the predominance of the capture to the $m = 0$ state at high energies. This later circumstance defines the high-energy limit of P [cf. Eqs. (13)–(16)] having the values of 0.6 for $2p\,^2P_{3/2}$–$1s\,^2S_{1/2}$, $3p\,^2P_{3/2}$–$2s\,^2S_{1/2}$ and $3d\,^2D_{3/2}$–$2p\,^2P_{1/2}$ transitions and 0.5 for the $3d\,^2D_{5/2}$–$2p\,^2P_{3/2}$ transition, respectively. We finally note that,

except for the $2p\ ^2P_{3/2}$–$1s\ ^2S_{1/2}$ transition with $r_d \geqslant 6a_0$ and $3d\ ^2D_{5/2}$–$2p\ ^2P_{3/2}$ and $3d\ ^2D_{3/2}$–$2p\ ^2P_{1/2}$ transitions for $r_d = 6a_0$, the polarization degree becomes negative at low collision energies.

ACKNOWLEDGMENTS

This work was supported by the National Natural Science Foundation of China (Grants No. 10875017, No. 10904006, No. 11004014, and No. 10734140).

[1] S. Schippers, P. Boduch, J. van Buchem, F. W. Bliek, R. Hoekstra, R. Morgenstern, and R. E. Olson, J. Phys. B **28**, 3271 (1995).
[2] C. Laulhé, E. Jacquet, G. Cremer, J. Pascale, P. Boduch, G. Rieger, D. Lecler, M. Chantepie, and J. L. Cojan, Phys. Rev. A **52**, 3803 (1995).
[3] D. M. Gauntt and K. Danzmann, Phys. Rev. A **46**, 5580 (1992).
[4] E. Jacquet, H. Kucal, V. Bazin, P. Boduch, M. Chantepie, G. Cremer, C. Laulhé, D. Lecler, and J. Pascale, Phys. Rev. A **62**, 022712 (2000).
[5] C. Laulhé, E. Jacquet, P. Boduch, M. Chantepie, G. Cremer, N. Ghérardi, X. Husson, D. Lecler, and J. Pascale, J. Phys. B **30**, 1517 (1997).
[6] C. Laulhé, E. Jacquet, G. Cremer, J. Pascale, P. Boduch, G. Rieger, M. Chantepie, and D. Lecler, Phys. Rev. A **55**, 1088 (1997).
[7] T. Hayakawa, R. A. Lomsadze, C. Verzani, H. Watanabe, H. Tanuma, B. D. DePaola, and N. Kobayashi, Phys. Scr., T **92**, 322 (2001).
[8] H. Tanuma, T. Hayakawa, C. Verzani, H. Kano, H. Watanabe, B. D. DePaola, and N. Kobayashi, J. Phys. B **33**, 5091 (2000).
[9] L. Liu, Y. Q. Zhao, J. G. Wang, R. K. Janev, and H. Tanuma, Phys. Rev. A **81**, 014702 (2010).
[10] S. Schippers, P. Boduch, J. van Buchem, F. W. Bliek, R. Hoekstra, R. Morgenstern, and R. E. Olson, J. Phys. B **28**, 3271 (1995).
[11] C. G. Kim and Y. D. Jung, Phys. Plasmas **5**, 2806 (1998).
[12] N. Bohr and J. Lindhard, K. Dan. Vidensk. Selsk. Mat. Fys. Medd. **28**, 1 (1954).
[13] H. Zhang, J. G. Wang, B. He, Y. B. Qiu, and R. K. Janev, Phys. Plasmas **14**, 053505 (2007).
[14] S. L. Zeng, L. Liu, J. G. Wang, and R. K. Janev, J. Phys. B **41**, 135202 (2008).
[15] L. Liu, J. G. Wang, and R. K. Janev, Phys. Rev. A **77**, 032709 (2008).
[16] L. Liu, J. G. Wang, and R. K. Janev, Phys. Rev. A **77**, 042712 (2008).
[17] L. Liu, J. G. Wang, and R. K. Janev, Phys. Rev. A **79**, 052702 (2009).
[18] L. D. Landau and E. M. Lifshitz, *Quantum Mechanics: Non-Relativistic Theory* (Pergamon, London, 1958).
[19] W. Fritsch and C. D. Lin, Phys. Rep. **202**, 1 (1991).
[20] C. M. Reeves, J. Chem. Phys. **39**, 1 (1963).
[21] U. Fano and J. H. Macek, Rev. Mod. Phys. **45**, 553 (1973).
[22] J. Kuang and C. D. Lin, J. Phys. B **30**, 101 (1997).
[23] B. H. Bransden and M. R. C. McDowell, *Charge Exchange and the Theory of Ion-Atom Collisions* (Clarendon Press, Oxford, 1992).
[24] T. S. Ho, R. Umberger, R. L. Day, M. Lieber, and F. T. Chan, Phys. Rev. A **24**, 705 (1981).
[25] A. Salin, J. Physique **45**, 671 (1984).